Push-pull dyes based on Michler's aldehyde: Design and characterization of the optical and electrochemical properties

Corentin Pigot, Sébastien Péralta, Thanh-Tuân Bui, Malek Nechab, Frédéric Dumur

Push-pull dyes based on Michler's aldehyde: Design and characterization of the optical and electrochemical properties

Corentin Pigot [1,*], Sébastien Péralta [2], Thanh-Tuân Bui [2], Malek Nechab[1] and Frédéric Dumur [1,*]

[1] Aix Marseille Univ, CNRS, ICR UMR7273, F-13397 Marseille France
[2] CY Cergy Paris Université, LPPI, F-95000 Cergy, France

* Correspondence: corentin.pigot@univ-amu.fr, frederic.dumur@univ-amu.fr

Abstract

Fifteen dyes based on Michler's aldehyde used as the electron donating group and differing by the electron accepting groups have been designed and synthesized. Interestingly, all dyes showed a broad absorption extending over the visible range. Examination of the solvatochromism in twenty-three solvents of different polarities revealed these dyes to give remarkable linear correlations using the Kamlet-Taft solvent polarity scale or the SPP Catalan empirical scales. The different dyes were also characterized by photoluminescence spectroscopy as well as cyclic voltammetry. To get a deeper insight into the optical properties of the different dyes, theoretical calculations were also carried out.

Keywords:

Push-pull dyes, solvatochromism, Michler's aldehyde, TNF, TCF, rhodanine

Introduction

Push-pull dyes that comprise an electron donor connected to an electron acceptor by mean of a spacer are the focus of intense research efforts due to the facile tunability of their optical properties. [1,2] By acting on the electron donating and the electron accepting abilities of the two partners, position of the intramolecular charge transfer band can be easily modified and dyes absorbing from the near-UV-visible range to the infrared region can be easily prepared. Jointly, broadness of the ICT band can also be enlarged by extending the π-conjugated spacer so that dyes with panchromatic absorptions are now accessible.[3–5] Benefiting from their intense absorption bands in the visible range, push-pull dyes thus constitute candidates of choice for applications such as dyes for non-linear optics,[6–8] active layers for solar cells,[9–15] biological labelling[16,17] organic field effect transistors[18–24] photochroms[25–29] or as

visible light photoinitiators of polymerization.[30–39] With aim at optimizing the synthetic routes of numerous organic compounds, recently, photoredox catalysis making used of push-pull dyes as photosensitizers has emerged as a promising approach which was applied to various chemical transformations.[40–43] Considering that the intramolecular charge transfer (ICT) band constitutes the key element of push-pull dyes focusing the interest of numerous researchers, intensity and position of this absorption band can be easily modified by applying the following principles. Notably, at constant electron acceptor, a red-shift of the ICT band can be obtained by elongating the spacer between the donor and the acceptor, but also by improving the electron-releasing ability of the donor.[44–52] Parallel to the red-shift, elongation of the spacer also mechanically induces an enhancement of the molar extinction coefficient by improving the oscillator strength.[53,54] Among electron donors that inherently comprise an elongated spacer, cinnamaldehydes are appealing candidates.[55] With aim at developing donors with electron donating abilities improved compared to that of 4-dimethylaminobenzaldehyde, Michler's aldehyde i.e. 3,3-*bis*(4-(dimethylamino) phenyl)acrylaldehyde is a cinnamaldehyde derivative exhibiting a strong electron donating ability. This aldehyde was notably at the basis of numerous dyes used for the design of chromophores for solar cells or photoinitiators of polymerization.[56–61]

In this work, a series of 15 dyes based on Michler's aldehyde have been prepared and examined for their photophysical properties (See Figure 1). Notably, a positive solvatochromism could be evidenced with several semi-empirical scales such as the Kamlet-Taft or the Catalan empirical scales. The different dyes were also examined for their electrochemical properties and theoretical calculations were carried out to support the experimental data. Besides, these dyes have been examined in five separated studies so that their optical properties were tested in different conditions. It has to be noticed that in this work, allylrhodamine (**EA14**) has been studied with ethylrhodanine (**EA13**) as electron acceptor precursors. Even if the replacement of an ethyl group by an allyl group is out of interest from the photophysical properties viewpoint, it can provide a unique opportunity to design dyes that can be used in the Future by photopolymerists. Indeed, Type II photoinitiators are extremely popular in photopolymerization and we wanted to anticipate future works of photopolymerists aiming at addressing the extractability issue.[32,62–72] **EA1-EA15** have been selected as electron acceptors as these structures strongly differ by their electron-withdrawing ability. Malononitrile (**EA1**) is a weak acceptor [73–76] whereas **EA8** is the strongest one of the series. The others offer a gradient of electron-withdrawing ability. To end, methyl pyridinium (**EA15**)

is commonly used as electron acceptor.[77–79] Therefore, considering the wide range of electron acceptor used, it was logical to include it in this study. Besides, we do agree that due to its betaine structure, its solvatochromism could be anticipated to be different from that of the other dyes.

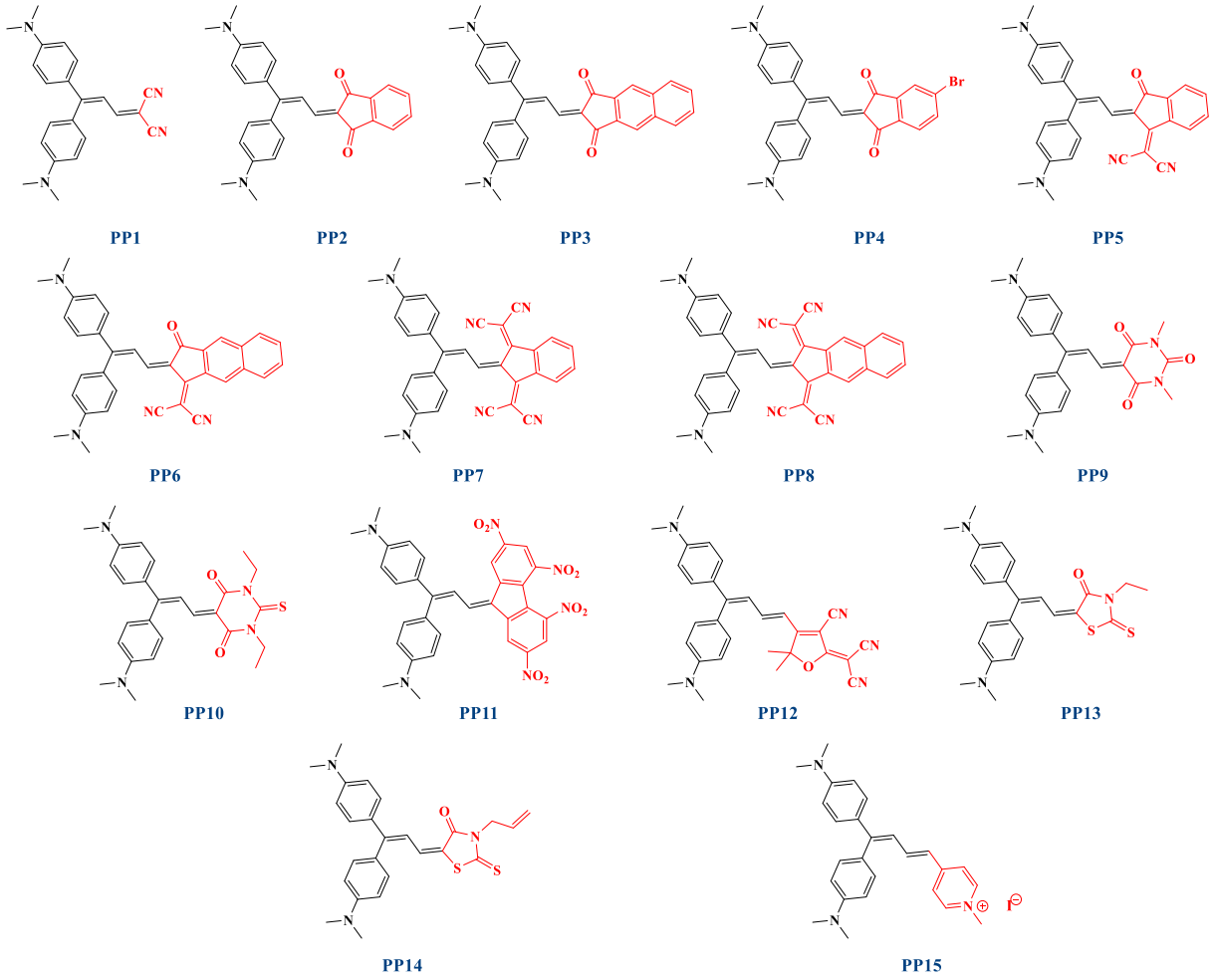

Figure 1. Chemical structures of push-pull dyes **PP1-PP15** examined in this work.

2. Results and Discussion

2.1. Synthesis of the dyes

The fifteen dyes reported in this work have been prepared by a Knoevenagel reaction between Michler's aldehyde and the different acceptor precursors. However, depending on the electron acceptors used, different synthetic conditions had to be used. Typically, Knoevenagel reactions are carried out in basic conditions, using piperidine[80,81] or diisopropylamine[82] as the bases. Thus, in the case of **EA1**, **EA3-EA6**, **EA9**, **EA10**, **EA12-EA15**, piperidine was

used as organocatalyst. Conversely, in the case of **EA2**, no base was used, the Knoevenagel reaction occurred spontaneously with the condensation of **EA2** in ethanol. **PP2** could be obtained in 85% yield. Similarly, by using a highly polar solvent such as DMF, **EA11** could spontaneously condensate, enabling to get **PP11** in 78% yield after 10 min. of reaction. Finally, in the case of **EA7** and **EA8**, due to the remarkable stability of **EA7** and **EA8** anions in basic conditions, these anions are totally unreactive for Knoevenagel reactions so that acidic coupling conditions had to be used. The two dyes were prepared by refluxing Michler's aldehyde and **EA7** or **EA8** in acetic anhydride overnight, enabling to get **PP7** and **PP8** in 89 and 84% yields. Overall, as shown in Scheme 1, **PP1**-**PP15** could be obtained with acceptable reaction yields ranging from 75% for **PP13** to 89% for **PP7**. It has to be noticed that among the fifteen dyes reported in this work, seven of them i.e. **PP4**, **PP6**, **PP8**-**PP10**, **PP13**, and **PP14** have never been previously reported in the literature. Concerning the other dyes, **PP1** and **PP2** have only been examined as visible light photoinitiators of polymerization and not for their optical and photophysical properties.[61] **PP3**[83], **PP5**,[56] **PP7**,[56] **PP11**,[84] **PP12**,[85] and **PP15**[86] have previously been synthesized and investigated for their optical properties. Michler's aldehyde has been prepared according the procedure developed by our group in 2008.[86]

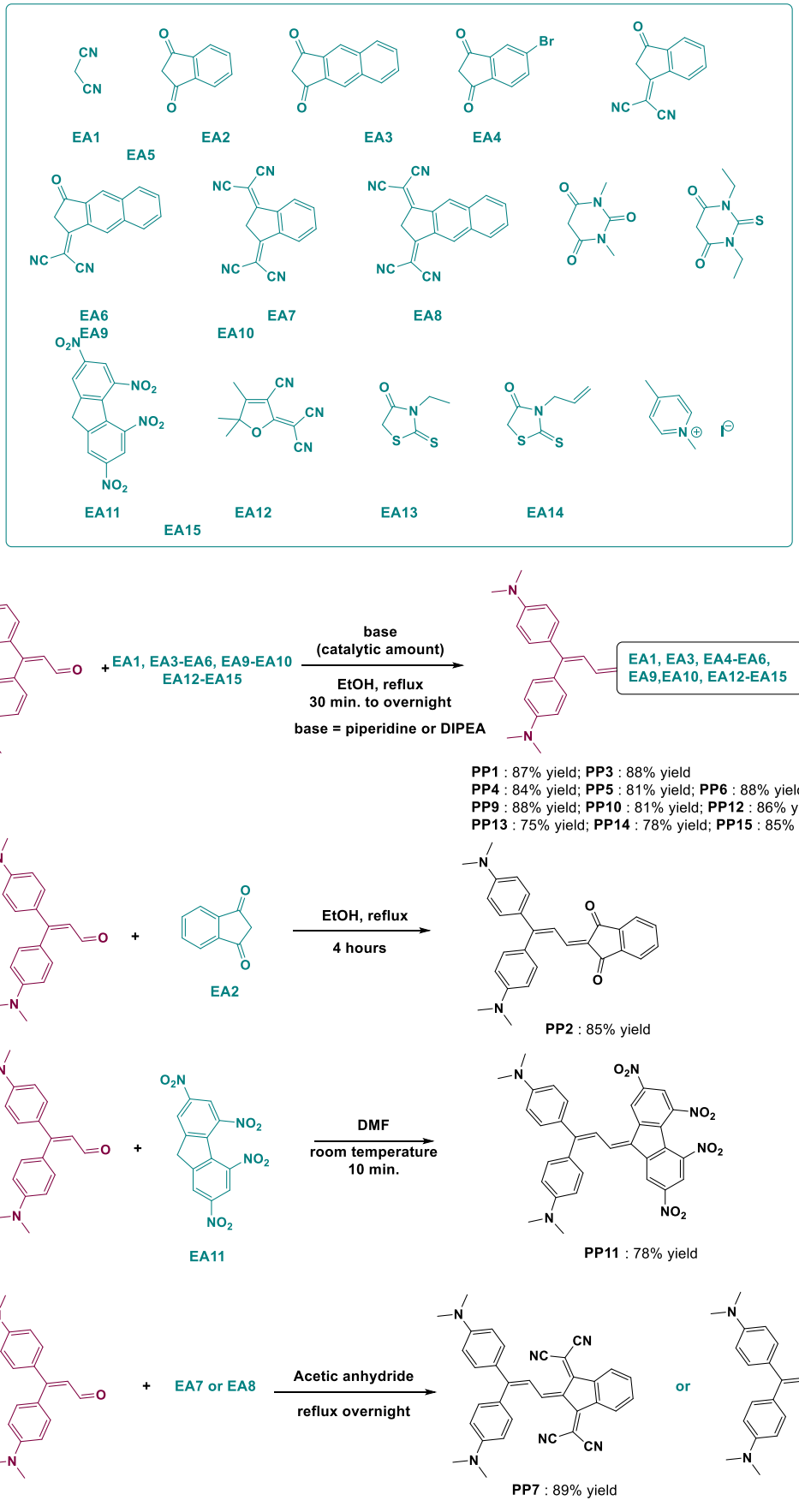

Scheme 1. Synthetic routes to **PP1-PP15**.

Noticeably, among the fifteen electron-acceptors used in this study, only six electron acceptors i.e. **EA1**, **EA2**, **EA9**, **EA10**, **EA13** and **EA14** are commercially available. All the other electron acceptors were prepared according to procedures previously reported in the literature (See SI). An original electron acceptor had notably to be prepared, namely 2,2'-(1*H*-cyclopenta[*b*]naphthalene-1,3(2*H*)-diylidene)dimalononitrile **EA8**. This electron acceptor could only be obtained from **EA3**[87] at elevated temperature, by using butan-1-ol as the solvent for the Knoevenagel reaction. Indeed, all attempts to prepare this electron acceptor in similar conditions to that used for **EA7**, namely by using sodium acetate as the base and ethanol as the solvent failed, only producing **EA6** as the unique reaction product. By using new reaction conditions, namely ammonium acetate[88–90] (that is sometimes used as the base for the synthesis of **EA7)** and butan-1-ol as the solvent, **EA8** could be obtained in 38% yield (See Scheme 2).

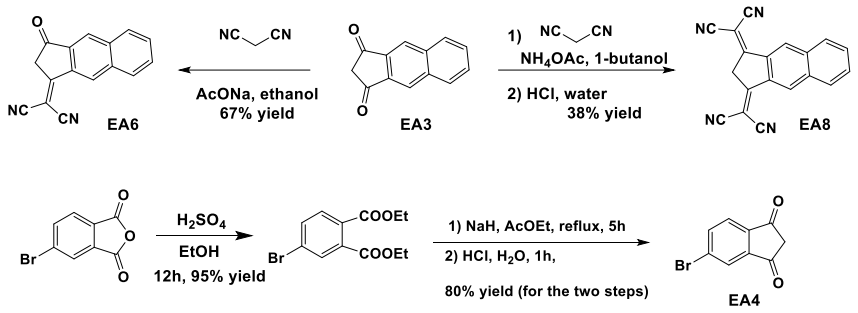

Scheme 2. Synthetic route to **EA4**, **EA6** and **EA8**.

Finally, an original synthetic route was also developed for the synthesis of 5-bromo-1*H*-indene-1,3(2*H*)-dione **EA4** even if the synthesis of this electron acceptor was previously reported in the literature.[91,92] Notably, 4-bromophthalic anhydride first reacted with ethanol in acidic conditions, enabling to produce diethyl 4-bromophthalate in almost quantitative yield. Then, in a second step, by mean of a Claisen condensation of the diester with ethyl acetate using NaH as the base, the intermediate sodium 5-bromo-2-(ethoxycarbonyl)-1,3-dioxo-2,3-dihydro-1*H*-inden-2-ide could be formed. Upon treatment under acidic conditions, the targeted 5-bromo-1*H*-indene-1,3(2*H*)-dione **EA4** could be obtained in 80% for the two steps (See Scheme 2).

2.2. Optical properties

Due to the good solubility of all dyes in chloroform, comparison of their optical properties was carried out in this solvent. It has to be noticed that the photoluminescence of the different dyes has not reported in this work, the dyes being not emissive at all. As shown in

Figure 2, all dyes showed a broad absorption band in the visible range corresponding to the intramolecular charge transfer (ICT) band. As anticipated, the most blue-shifted absorption (λ_{max} = 500 nm) was detected for **PP1** exhibiting malononitrile as the electron acceptor. The most red-shifted absorption was found for **PP8** exhibiting the strongest electron acceptor i.e. **EA8**. A maximum absorption located at 727 nm was found for this dye. Following this dye, the second most red-shifted absorption was logically found for **PP7** (λ_{max} = 698 nm), also bearing a tetracyano-substituted electron acceptor (**EA7**) but differing from **EA8** by its polyaromaticity. Interestingly, **PP11** showed two ICT bands located in the visible range at 557 and 696 nm respectively and presence of these two ICT bands are consistent with previous results reported in the literature for dyes comprising 2,4,5,7-tetranitro-9*H*-fluorene **EA11** as the acceptor.[84,93] Noticeably, all dyes exhibited a second intense absorption band close to the ICT band appearing as a second absorption band such as in the case of **PP7** and **PP8**, or a shoulder such as in **PP3** and **PP4**. Based on theoretical calculations later detailed in the manuscript but also in SI, this second absorption band detected at higher energy than the ICT band can be assigned to HOMO-1 => LUMO or HOMO => LUMO+1 transitions, depending on the dye. Especially, two absorption bands with high oscillator strength could be determined for all dyes. **PP1-PP15** are also characterized by remarkable molar extinction coefficients and the results are summarized in Table 1. As shown in Figure 3, all dyes exhibited high molar extinction coefficients. The smallest molar extinction coefficient was found for **PP11** comprising the TNF acceptor. A molar extinction coefficient of 28150 $M^{-1}.cm^{-1}$ was found for this dye at 557 nm. The highest molar extinction coefficients were determined for **PP7** and **PP8** comprising respectively 2,2'-(1*H*-indene-1,3(2*H*)-diylidene)dimalononitrile **EA7** and 2,2'-(1*H*-cyclo-penta[*b*]naphthalene-1,3(2*H*)-diylidene)dimalononitrile **EA8** as the acceptor, the molar extinction coefficients peaking respectively at 97950 and 89200 $M^{-1}.cm^{-1}$ for **PP7** and **PP8**.

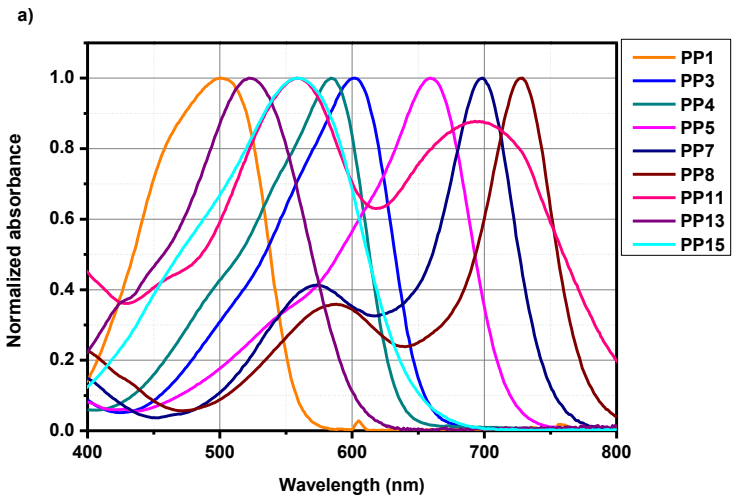

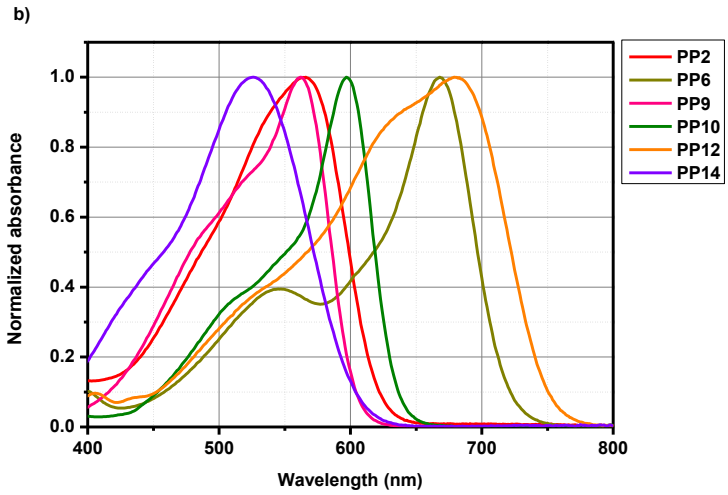

Figure 2. Normalized UV-visible absorption spectra of **PP1-PP15** in chloroform.

This is directly related to the strong electronic delocalization involved by these two electron acceptors. Comparison of the absorption maxima also revealed **EA2** to exhibit similar electron-withdrawing ability as **EA15**, positions of the ICT bands for **PP2** and **PP15** being respectively detected at 571 and 572 nm. Similarly, comparable positions of the ICT bands were found for **PP6**, **PP7** and **PP11**, the absorption maxima being found at 697, 698 and 693 nm respectively. Besides, from a chemical architecture viewpoint, the three electron-acceptors **EA6**, **EA7** and **EA11** drastically differs. Indeed, if **EA6** is a dicyano-substituted polyaromatic structure, **EA7** is a tetracyano-substituted electron acceptor and **EA11** a tetranitro-substituted one. Similarly, **PP3** and **PP10** exhibited absorption maxima at 606 and 598 nm respectively. Overall, considering that the same electron donor has been used for the design of the different dyes, a classification of the electron acceptors can be done, based on the positions of the ICT bands (See Figure 4). As shown in Figure 4, if malononitrile constitutes the weakest electron acceptor of the series, undoubtedly, 2,2'-(1*H*-cyclo-penta[*b*]naphthalene-1,3(2*H*)-diylidene)dimalononitrile **EA8** is the strongest electron acceptor even outperforming 2,4,5,7-tetranitro-9*H*-fluorene (TNF, **EA11**). However, it has to be noticed that all electron acceptors don't exhibit the same polyaromaticity. Consequently, position of the ICT band is also dependent of the degree of conjugation of the whole compounds and the number of π-electrons involved in the different systems. Therefore, the classification of electron acceptors presented in the Figure 4 is only based on the positions of the ICT bands determined for a series of dyes based on the same electron donor. Even if not fully correct, it nevertheless gives interesting trends helping to design push-pull dyes, especially for chemists who want to design dyes absorbing at 400 or 800 nm, while using the same electron donor.

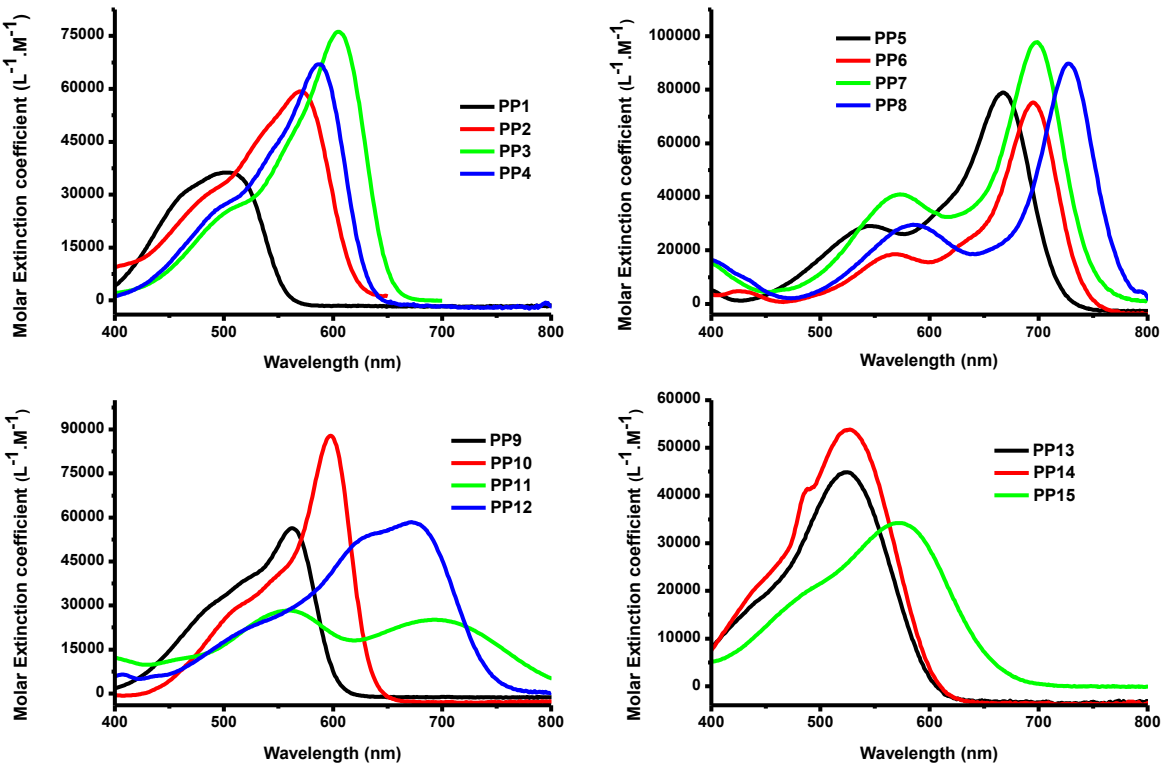

Figure 3. UV-visible absorption spectra of **PP1-PP15** in chloroform.

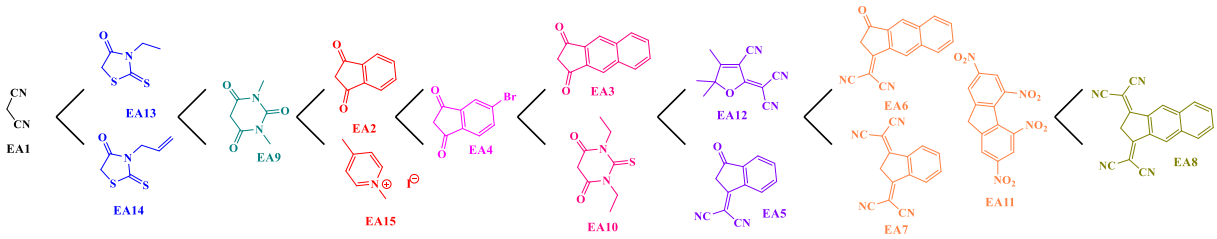

Figure 4. Classification of electron acceptors established on the basis of the experimental position of the absorption maxima.

Theoretical studies were also carried out to investigate the energy levels as well as the molecular orbitals (M.O.) compositions of the different dyes. DFT calculations were performed for all dyes at the B3LYP/6-311G(d,p) level of the theory using Gaussian 09 programs except for **PP15** for which the LAND2Z basis set was used to determine the transitions involved in the different absorption peaks. Chloroform was used as the solvent model with a polarizable continuum model (PCM).[94–100] As shown in Table 1 and Figure 5, a blue-shift of the theoretical absorption spectra was found for all dyes compared to the experimental ones.

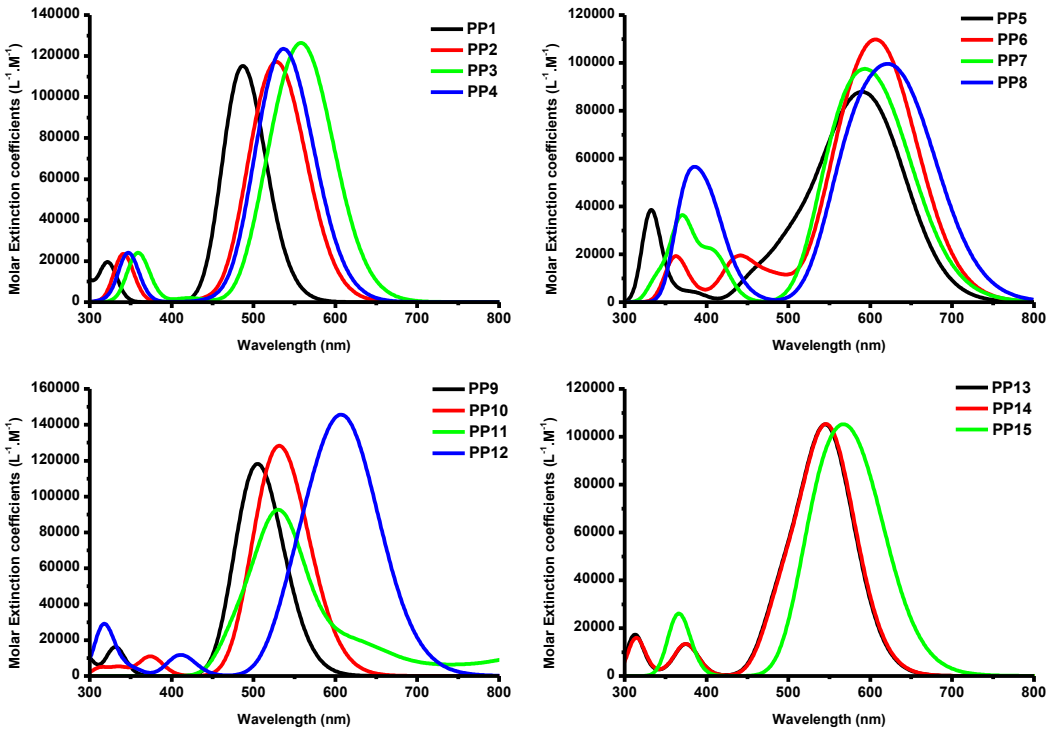

Figure 5. Theoretical UV-visible absorption spectra of **PP1-PP15** in chloroform.

Typically, a difference of about 30 nm was found between the experimental and the theoretical absorption maxima. This difference increased up to 105 nm, 110 nm and 160 nm for **PP7**, **PP8** and **PP11** respectively. Concerning **PP11**, mismatch between the experimental and theoretical values was already reported for TNF-based push-pull dyes and assigned to the difficulty to model the UV-visible absorption spectra of these dyes exhibiting two ICT bands.[84] Concerning **PP7** and **PP8**, the mismatch between the experimental and theoretical absorption spectra can originate from the torsion induced by the presence of the two dicyanomethylene groups on **EA7** and **EA8**, resulting from the steric hindrance generated by these groups with the electron donor.

Table 1. Optical characteristics of the different compounds in chloroform and the values theoretically determined.

chloroform								
compounds	**PP1**	**PP2**	**PP3**	**PP4**	**PP5**	**PP6**	**PP7**	**PP8**
λ (nm)	503	571	606	587	543, 670	568, 697	572, 698	587, 727
ϵ ($M^{-1}.cm^{-1}$)	36400	58800	75900	66600	28900, 77950	18350, 74700	40900, 97950	28900, 89200
Δ E(eV)	2.46	2.17	2.05	2.11	1.85	1.78	1.78	1.70
compounds	**PP9**	**PP10**	**PP11**	**PP12**	**PP13**	**PP14**	**PP15**	
λ (nm)	560	598	557, 693	674	523	527	572	
ϵ ($M^{-1}.cm^{-1}$)	55900	86900	28150,	58120	44400	53900	34200	

			25150					
Δ E(eV)	2.21	2.07	1.79	1.84	2.37	2.35	2.17	

Theoretical values in chloroform								
compounds	**PP1**	**PP2**	**PP3**	**PP4**	**PP5**	**PP6**	**PP7**	**PP8**
λ (nm)	487	529	558	536	589	606	593	619
ϵ ($M^{-1}.cm^{-1}$)	115000	116000	126500	122500	87600	110000	98200	99000
Δ E(eV)	2.54	2.34	2.22	2.31	2.10	2.04	2.09	2.00
compounds	**PP9**	**PP10**	**PP11**	**PP12**	**PP13**	**PP14**	**PP15**	
λ (nm)	506	531	530	606	545	545	565	
ϵ ($M^{-1}.cm^{-1}$)	118000	128000	93000	145000	106000	106000	105000	
Δ E(eV)	2.45	2.33	2.33	2.05	2.45	2.45	2.19	

While examining the composition of the ICT band detected in the visible, as shown in Table 2, this absorption band is mainly associated to HOMO->LUMO, HOMO-1->LUMO and HOMO-> LUMO+1 transitions, depending on the dye. Even if a mismatch is observed between the experimental and theoretical positions of the ICT bands, a clear trend can be observed. Thus, by improving the electron deficiency of the electron acceptor, a red-shift of the absorption maxima can be observed, the most red-shifted absorption being observed for the strongest electron acceptor of the series, namely **EA8**. Second, within this series of dyes, if the HOMO level remains relatively constant, the electron donor being the same for all dyes, as anticipated, improvement of the electron withdrawing ability of the acceptors resulted in a stabilization of the LUMO energy level, decreasing from -2.61 eV for **PP1** to -3.24 eV for **PP8**. Besides, another explanation can also be given. Indeed, the maximum absorbance wavelength depends on the degree of conjugation, especially when HOMO -> LUMO dominates the ICT. The HOMO-LUMO gap energy will decrease with the increase of the strength of the electron-withdrawing group, but also with increasing the number of electrons in the ICT molecular pathway. Both structural features increase the conjugation, reducing the HOMO-LUMO gap, and ultimately shifting the absorption band bathochromically. Therefore, the relative position of the maximum absorbance wavelength cannot be attached solely to the electron-withdrawing strength of the acceptor moiety, neglecting the fact that the number of electrons participating in the solvatochromic core of the dyes is not constant or nearly constant. Therefore, the results can be explained in terms of conjugation, and not only in terms of electron-withdrawing ability. For instance, as shown in Figure 6, the naphthalene subunit of **PP8** has an essential participation in the ICT. While examining the electronic distribution of the HOMO and LUMO energy levels, a localization of the HOMO energy level mostly located onto the electron donor and a LUMO

energy level mostly centered onto the electron acceptor was logically observed, as shown in Figure 6.

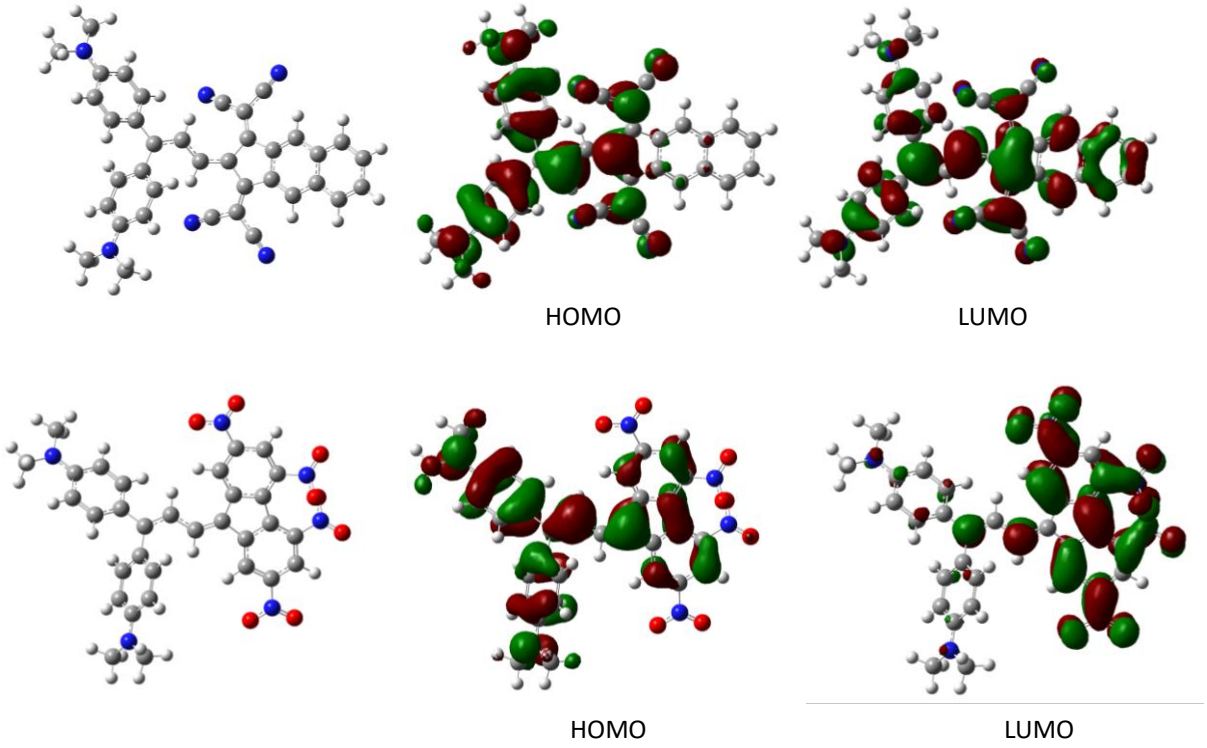

Figure 6. Contour plots of the HOMO and LUMO energy levels for **PP8** and **PP11**.

Table 2. Summary of the simulated absorption characteristics in dilute chloroform of synthetized compounds. Data were obtained in chloroform solution. Position of the HOMO and LUMO energy levels determined by electrochemistry in acetonitrile are also given. Optical, electrochemical and theoretical bandgaps are given in eV.

Compounds	$E_{HOMO\ (th)}$ (eV)	$E_{LUMO\ (th)}$ (eV)	λ_{max} (nm)	Transitions	$E_{HOMO\ (el)}$ (eV)	$E_{LUMO\ (el)}$ (eV)	ΔE_{TH}[a] (eV)	ΔE_{ET}[b] (eV)	ΔE_{opt}[c] (eV)	ΔE_{opt}[d] (eV)
PP1	-5.53	-2.74	501	HOMO-1=>LUMO (53%)	-5.18	-3.50	2.79	1.68	2.46	2.51
PP2	-5.39	-2.77	540	HOMO=>LUMO (89%)	−5.16	−3.55	2.62	1.70	2.17	2.23
PP3	-5.41	-2.90	569	HOMO=>LUMO (93%)	−5.17	−3.55	2.51	1.62	2.05	2.08
PP4	-5.44	-2.85	550	HOMO=>LUMO (88%)	-5.16	-3.53	2.59	1.63	2.11	2.14
PP5	-5.49	-3.12	613	HOMO=>LUMO (91%)	-5.09	-3.60	2.37	1.49	1.85	1.87
PP6	-5.50	-3.18	624	HOMO=>LUMO (93%)	- 5.17	-3.70	2.32	1.47	1.78	1.86
PP7	-5.60	-3.26	652	HOMO=>LUMO (91%)	-5.17	-3.90	2.34	1.39	1.77	1.78
PP8	-5.60	-3.30	644	HOMO=>LUMO (95%)	-5.10	-3.65	2.30	1.45	1.70	1.70
PP9	-5.46	-2.74	520	HOMO=>LUMO (75%)	-5.12	-3.59	2.72	1.53	2.21	2.27
PP10	-5.50	-2.89	546	HOMO=>LUMO (85%)	-5.18	-3.67	2.61	1.51	2.07	2.10
PP11	-5.54	-3.79	914	HOMO=>LUMO (98%)	-5.14	-4.02	1.75	1.35	1.79	1.82
PP12	-5.42	-3.17	616	HOMO=>LUMO (94%)	-5.09	-3.88	2.25	1.21	1.84	1.92
PP13	-5.24	-2.69	548	HOMO=>LUMO (98%)	-5.02	-3.67	2.55	1.35	2.37	2.42
PP14	-5.25	-2.71	549	HOMO=>LUMO (98%)	-5.00	-3.73	2.54	1.27	2.35	2.41
PP15	-5.16	-2.84	649	HOMO=>LUMO (84%)	-5.10	-3.63	2.32	1.47	2.17	2.22

[a] ΔE_{TH} in chloroform [b] ΔE_{ET} in acetonitrile [c] ΔE_{opt} in chloroform. [d] ΔE_{opt} in acetonitrile.

2.3. Solvatochromism

Push-pull dyes typically exhibit a strong sensitivity to the solvent polarity so that influence of this parameter on the optical properties was examined in twenty-three solvents of different polarities. Intramolecular character of the charge transfer process was confirmed by examining the variation of the optical density with the concentration. All dyes showed linear correlations upon dilution of the different solutions, excluding the presence of intermolecular interactions between dyes.[101] To get a deeper insight into the solvatochromism, several empirical polarity scales have been developed and the Kamlet-Taft's,[102] Catalan's,[103] Kawski-Chamma Viallet's,[104] Lippert-Mataga's,[105] McRae Suppan's,[106] Dimroth-Reichardt's,[107] and Bakhshiev's[108] scales are well adapted for push-pull dyes exhibiting D-π-A structures.[109,110] A summary of the optical properties is provided in Tables 3 and 4.

Table 3. Summary of the optical properties of **PP1-PP8** in solvents of different polarities.

compounds	**π*[1]**	**PP1[2]**	**PP2[2]**	**PP3[2]**	**PP4[2]**	**PP5[2]**	**PP6[2]**	**PP7[2]**	**PP8[2]**
heptane	-0.08	461	n.s.[3]	551	537	625	625	n.s.[3]	689
cyclohexane	0.00	465	525	555	543	630	633	666	766
triethylamine	0.14	469	n.s.[3]	561	546	638	n.s.[3]	n.s.[3]	n.s.[3]
diethyl ether	0.27	475	533	569	555	645	645	n.s.[3]	734
p-xylene	0.43	483	550	579	564	649	649	688	715
diethyl carbonate	0.45	479	533	576	558	648	644	684	714
AcOEt	0.54	483	550	581	567	656	653	687	721
butanol	0.47	492	578	614	590	668	667	n.s.[3]	727
ethanol	0.54	497	578	616	590	667	668	n.s.[3]	726
toluene	0.54	487	550	584	567	653	652	682	716
1,4-dioxane	0.55	481	544	578	560	648	647	n.s.[3]	716
THF	0.58	490	553	588	567	665	659	692	725
diglyme	0.64	496	556	594	579	672	669	698	732
acetone	0.71	492	562	594	576	666	667	697	727
anisole	0.73	500	564	598	581	667	664	699	730
acetonitrile	0.75	493	555	595	578	663	665	696	727
chloroform	0.78	500	566	602	584	659	668	699	729
1,2-dichloroethane	0.81	500	557	575	569	651	667	699	729
dichloromethane	0.82	500	573	605	584	668	668	699	728
dimethylacetamide	0.88	504	575	607	591	682	682	709	740
DMF	0.87	505	569	610	591	680	679	706	740
DMSO	1.00	514	583	620	600	687	686	713	743
nitrobenzene	1.01	520	582	617	599	685	687	712	743

[1] Kamlet and Taft parameters [2] Position of the ICT bands are given in nm. n.s.[3] : not soluble.

Table 4. Summary of the optical properties of **PP9-PP15** in solvents of different polarities.

compounds	π*[1]	PP9[2]	PP10[2]	PP11[2]	PP12[2]	PP13[2]	PP14[2]	PP15[2]
heptane	-0.08	511	549	n.s.[3]	n.s.[3]	481	483	n.s.[3]
cyclohexane	0.00	513	551	n.s.[3]	583	485	487	n.s.[3]
triethylamine	0.14	520	562	650	587	490	492	n.s.[3]
diethyl ether	0.27	518	569	n.s.[3]	602	495	502	497
p-xylene	0.43	530	577	662	605	506	507	n.s.[3]
diethyl carbonate	0.45	527	573	648	605	500	504	506
butanol	0.47	562	598	676	690	515	512	533
AcOEt	0.54	534	580	665	614	503	507	504
ethanol	0.54	562	598	676	697	514	517	529
toluene	0.54	533	578	667	609	508	509	526
1,4-dioxane	0.55	533	576	n.s.[3]	605	504	506	510
THF	0.58	537	583	676	627	512	512	516
diglyme	0.64	541	591	682	652	515	520	518
acetone	0.71	541	588	679	642	509	515	517
anisole	0.73	546	590	696	653	519	522	535
acetonitrile	0.75	546	591	681	644	512	515	515
chloroform	0.78	562	597	697	673	522	526	558
1,2-dichloroethane	0.81	553	593	694	684	521	523	586
dichloromethane	0.82	557	595	697	679	520	524	576
dimethylacetamide	0.88	555	504	696	687	532	532	514
dimethylformamide	0.87	555	602	696	689	526	528	515
DMSO	1.00	563	609	692	707	534	536	512
nitrobenzene	1.01	567	606	722	706	538	541	565

[1] Kamlet and Taft parameters [2] Position of the ICT bands are given in nm. n.s.[3] : not soluble.

Interestingly, among the different polarity scales examined, good correlations could be obtained with the Kamlet-Taft and the Catalan polarity scales. As shown in Figure 7, remarkable linear correlations could be determined for **PP7**. The same holds true for all dyes except **PP11** and **PP12** for which lower squares for the correlation coefficients (R^2) could be determined. In the case of **PP15**, no linear correlations could be obtained, irrespective of the solvent polarity scales (See Figure 8). This unusual behaviour for pyridinium-based dyes has previously been reported in the literature for betaine dyes and assigned to a modification of the relative electrophilicities of both the electron-pair donor and acceptor moieties with the solvent, so that irregular behaviours can be found for this family of dyes.[111–113] Besides, by using a multiparametric approach, better correlations could be obtained for **PP15**, since a correlation coefficient of 0.61 could be determined using the Catalan scale. The Catalan solvent polarity scale is also capable to discriminate between the solvent polarity/polarizability effect i.e. with the solvent polarity/polarizability (SPP) parameter and the solvent dipolarity effect, which is

examined with the solvent dipolarity (SdP) parameter. Based on the squares of the correlation coefficients, better linear regressions were obtained with the SPP parameter than the SdP one, evidencing that the solvatochromism was mainly governed the polarity/polarizability of the solvents.

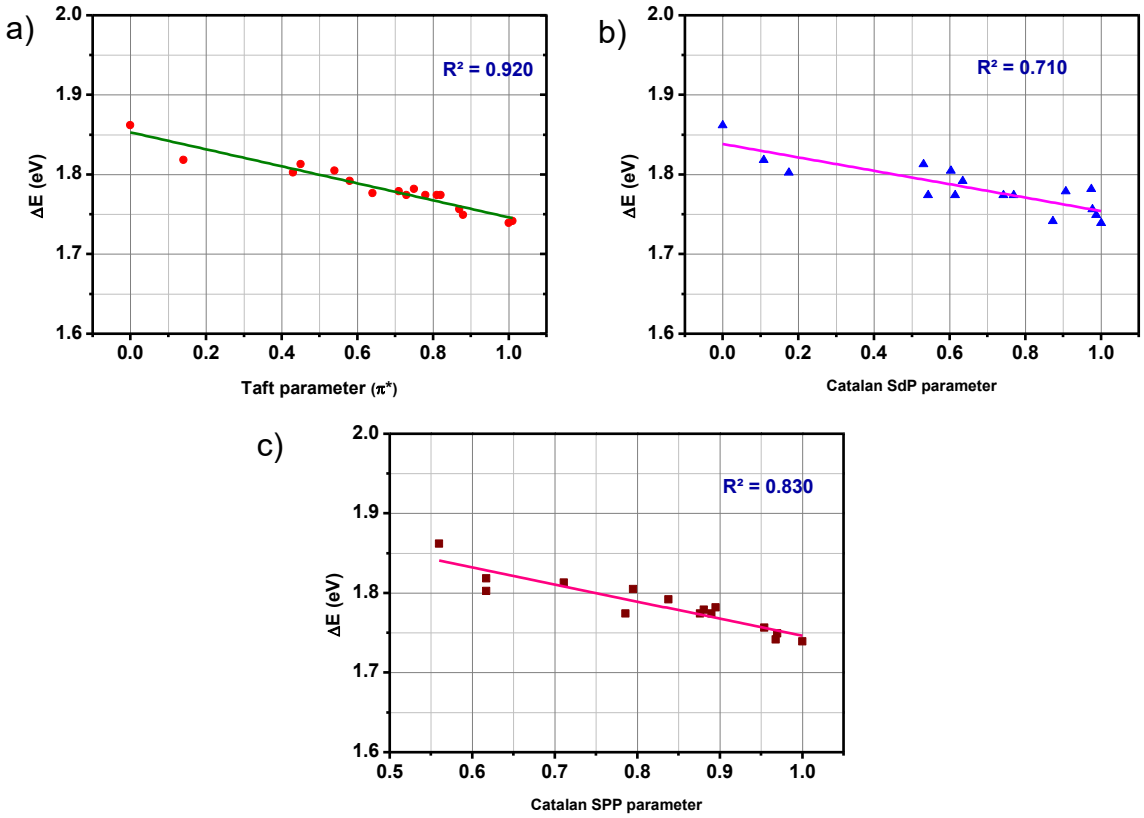

Figure 7. Linear correlations obtained while using different polarity scales for **PP7** Kamlet-Taft (a) and Catalan (b) and (c) empirical scales.

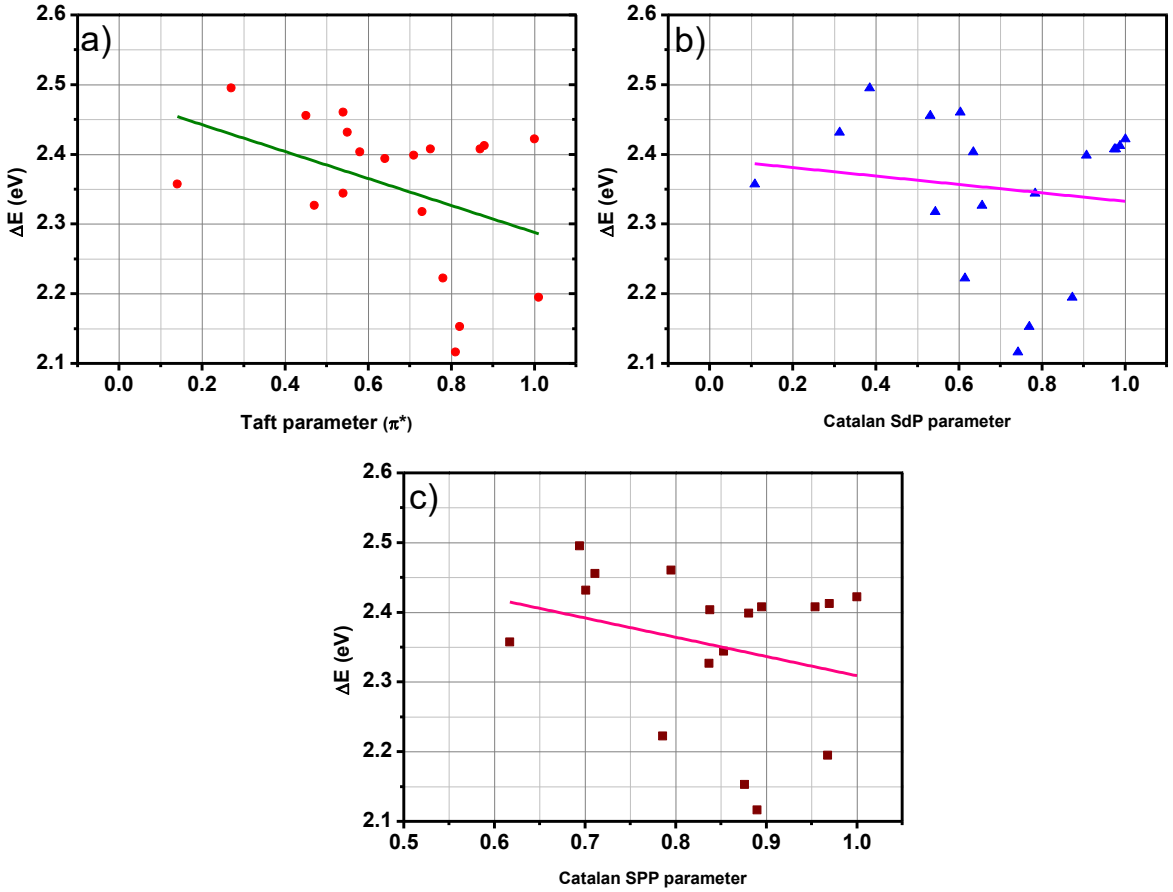

Figure 8. Linear correlations obtained while using different polarity scales for **PP15** Kamlet-Taft a) and Catalan b) and c) empirical scales.

Finally, sensitivity of the dyes to the solvent polarity was examined by plotting the variation of the HOMO-LUMO gaps vs. Taft parameters. As shown in Figure 9, similar slopes were found for all dyes, except **PP12** comprising a TCF electron acceptor. In this case, a greater slope was found, evidencing a higher charge redistribution upon photoexcitation.

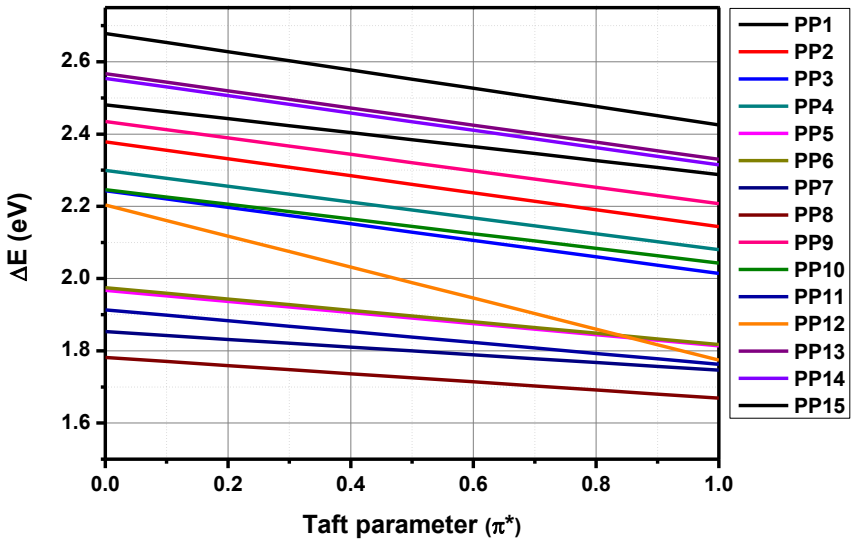

Figure 9. Variation of the HOMO-LUMO gaps of **PP1-PP15** with the solvent polarity using Taft parameters (π*).

2.4. Electrochemical properties

Electrochemical properties of **PP1-PP15** were measured in acetonitrile by cyclic voltammetry, at a scan rate of 100 $mV.s^{-1}$, using tetrabutylammonium hexafluorophosphate (0.1M) as the supporting electrolyte. The working, pseudo-reference and counter electrodes were platinum disk (Ø = 1 mm), Ag wire, and Au wire gauze, respectively. Ferrocene was used as an internal standard. Redox potentials of all dyes against the half-wave oxidation potential of the ferrocene/ferrocenium cation pair are given in Table 5. Along with the redox values, energy levels of the HOMO and LUMO orbitals are given, the values being determined by using the two equations established by Pommerehne et al.[114] Two cyclic voltammograms are also presented in Figure 10, the cyclic voltammogram of **PP4** containing ferrocene used as reference for calibration. In this work, all dyes possess the same electron donating group but differ by the electron accepting moieties. As shown in Table 5, all dyes exhibited a one-electron oxidation process around 0.40 V/Fc range except for **PP13** and **PP14** that comprise a rhodanine electron accepting moiety. In this case, an oxidation potential lowered by ca 200 mV was detected. As shown by DFT calculations, a high electronic density is located on the sulfur atoms of the rhodanine moiety so that the first oxidation process occurs on the sulfur atoms of the acceptor and not on the electron donating moiety. This behavior has previously been reported in the literature for rhodanine-based dyes comprising an electron donor of similar structure.[83]

Conversely, this behavior is not observed for **PP10**, also comprising an electron accepting group bearing a sulfur atom.

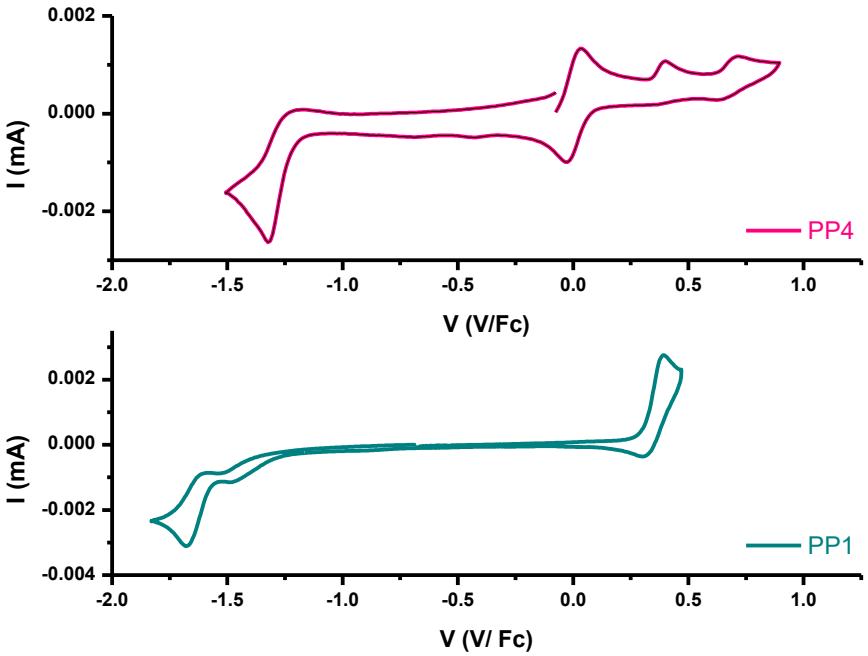

Figure 10. Comparisons between the cyclic voltammograms of **PP1** and **PP4** measured in acetonitrile at a scan rate of 100 $mV \cdot s^{-1}$, with tetrabutylammonium hexafluorophosphate ($TBAPF_6$) (0.1 M) as the supporting electrolyte (In the CV curve of **PP4**, redox system detected at 0V correspond to ferrocene used as a reference).

For all the other dyes, the similarity of the oxidation processes is consistent with an oxidation process centered on the dimethylamino group of the Michler's donor. Concerning the reduction process, logically, a decrease of the reduction potential with the electron accepting strength was observed. Thus, in the case of **PP1** comprising a weak electron acceptor, the reduction was determined at -1.48 V/Fc. Conversely, 2,4,5,7-tetranitrofluorene (TNF) used in **PP11** is among the strongest electron acceptor ever reported in the literature.[93] Due to its remarkable electron accepting ability, the dye could reduce at -0.89V/Fc. Similarly, 2-(3-cyano-4,5,5-trimethylfuran-2(5*H*)-ylidene)malononitrile (TCF) is a strong electron acceptor so that the reduction process of **PP12** could be detected at -1.13 V/Fc.[85] Interestingly, upon introduction of cyano groups on the indanedione derivatives (**PP5**, **PP7** and **PP6** and **PP8**) a significant decrease of the reduction potentials was observed, consistent with an improvement of the electron-withdrawing ability of the corresponding electron acceptors.

Table 5. Electrochemical characteristics of studied compounds **PP1-PP15.**

	E_{red1}[a]	E_{red1} onset	E_{Ox1}[a]	E_{ox1} onset	E_{HOMO}	E_{LUMO}	ΔE_{ET}	ΔE_{opt}[b]	ΔE_{opt}[c]
	V/Fc	V/Fc	V/Fc	V/Fc	eV	eV	eV	eV	eV
PP1	-1.48	-1.30	0.40	0.38	-5.18	-3.50	1.68	2.46	2.51
PP2	-1.30	-1.25	0.40	0.36	-5.20[d]	-3.50 [d]	1.70	2.17	2.23
PP3	-1.30	-1.25	0.41	0.37	-5.17	-3.55	1.62	2.05	2.08
PP4	-1.32	-1.27	0.39	0.36	-5.16	-3.53	1.63	2.11	2.14
PP5	-1.35	-1.20	0.38	0.29	-5.09	-3.60	1.49	1.85	1.87
PP6	-1.25	-1.10	0.44	0.37	- 5.17	-3.70	1.47	1.78	1.86
PP7	-1.02	-0.92	0.37	-	-5.17[d]	-3.78[d]	1.39	1.77	1.78
PP8	-1.24	-1.15	0.40	0.30	-5.10	-3.65	1.45	1.70	1.70
PP9	-1.30	-1.21	0.43	0.32	-5.12	-3.59	1.53	2.21	2.27
PP10	-1.25	-1.13	0.46	0.38	-5.18	-3.67	1.51	2.07	2.10
PP11	-0.89	-0.78	0.46	0.34	-5.26[d]	-3.91[d]	1.35	1.79	1.82
PP12	-0.92	-1.05	0.37	0.29	-5.09	-3.88	1.21	1.84	1.92
PP13	-1.39	-1.13	0.31	0.22	-5.02	-3.67	1.35	2.37	2.42
PP14	-1.40	-1.24	0.30	0.20	-5.00	-3.73	1.27	2.35	2.41
PP15	-1.32	-1.17	0.43	0.30	-5.10	-3.63	1.47	2.17	2.22

[a] All potentials recorded in 0.1M TBAP/acetonitrile. E_{HOMO} (eV) = - 4.8 – E_{ox} onset and E_{LUMO} (eV) = -4.8 – E_{red} onset. [b] ΔE_{opt} in chloroform. [c] ΔE_{opt} in acetonitrile. [d] determined for the oxidation or the reduction peak due to the weak intensity of the peak not enabling to determine the position of the onset with accuracy.

From the cyclic voltammograms, energy levels of the HOMO and LUMO orbitals could be estimated, and a comparison with the values determined experimentally and by theoretical calculations could be established.[115] As shown in Figure 11, a good adequation between the experimental and the theoretical values of the HOMO energy levels of all dyes could be found, even if the values are slightly underestimated by cyclic voltammetry. A higher mismatch could be found between the experimental and the theoretical values of the LUMO energy levels. In all cases, position of the LUMO levels was overestimated by theoretical calculations compared

to the experimental ones. This mismatch can be assigned to the electronic distribution of their LUMO orbitals. Indeed, for most of the dyes, a strong contribution of the electron donating moiety to the LUMO orbitals can be found. In the case of **PP15**, as shown in SI, a strong contribution of the pyridinium moiety is only found in LUMO+1, the LUMO orbital extending all over the molecule.

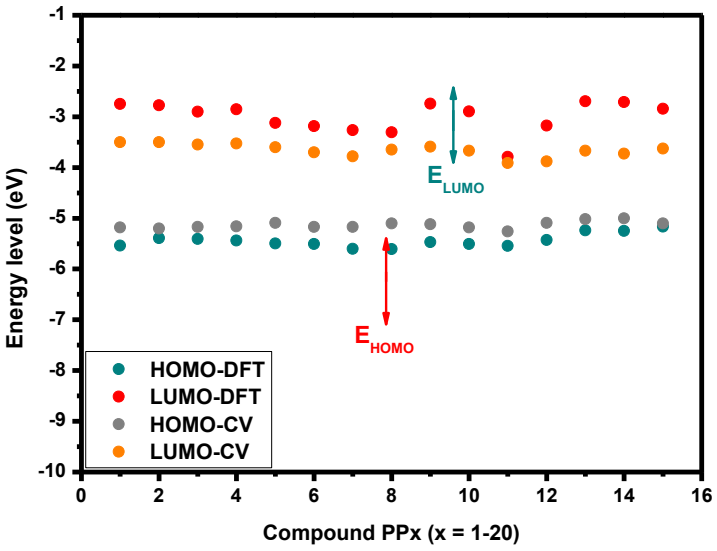

Figure 11. Comparisons between the frontier orbitals' energy levels estimated in chloroform by DFT calculations and those obtained by cyclic voltammetry in acetonitrile.

Finally, a comparison between the optical, electrochemical and theoretical bandgaps could be established. As shown in Figure 12, a relatively good adequation between the optical and the theoretical bandgaps could be determined for all dyes. Conversely, the electrochemical bandgap is greatly underestimated. This underestimation can notably be assigned to the difficulty to clearly determine the onsets of the oxidation and the reduction peaks on the different voltammograms.

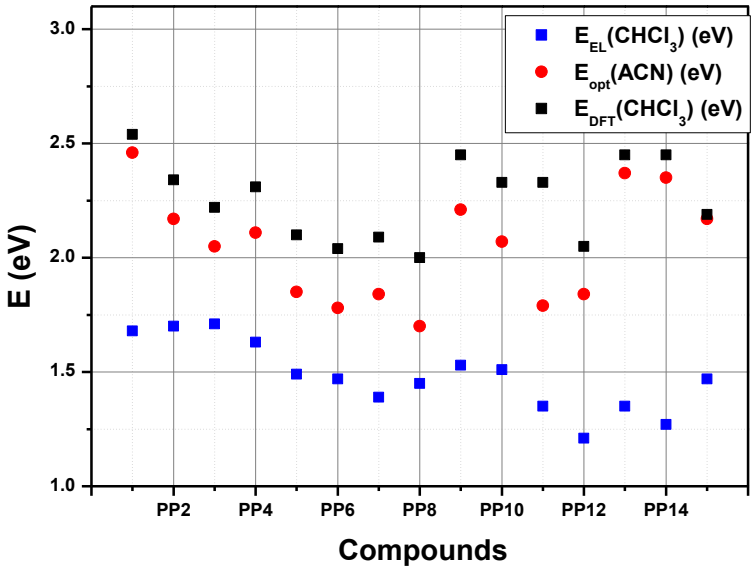

Figure 12. Comparisons of the bandgaps determined by UV-visible absorption spectroscopy in chloroform, cyclic voltammetry in acetonitrile and by theoretical calculations in chloroform.

Conclusion

In this work, a series of push-pull dyes based on Michler's donor have been studied using different techniques. Interestingly, by modifying the electron-withdrawing ability, dyes with absorption maxima located from 503 nm for **PP1** to 727 nm for **PP8** could be determined in chloroform. In this work, a new electron acceptor outperforming the reported structures has also been synthesized, namely **EA8**. Especially, **EA8** showed higher electron-withdrawing ability than the well-established 2,4,7,8-tetranitrofluorene **EA11**. Considering that the same electron donor has been used for elaborating the different dyes, a scale of electron-withdrawing ability could be established between electron acceptors of different structures. Interestingly, all dyes exhibited a positive solvatochromism, what is classically observed for dyes possessing a strong electron donor such as Michler's aldehyde. Analysis of the energy bandgaps by electrochemistry, UV-visible absorption spectroscopy and theoretical calculations revealed a good adequation between the theoretical and optical bandgaps. Future works will consist in developing dyes of extended π-conjugation between the donor and the acceptor in order to get dyes strongly absorbing in the near-infrared range. **EA8** being a new electron acceptor of unprecedented electron-withdrawing ability, future works will also consist in designing new dyes with this electron acceptor.

Acknowledgment

The authors thank Aix Marseille University and The Centre National de la Recherche Scientifique (CNRS) for financial supports. The Agence Nationale de la Recherche (ANR agency) is acknowledged for its financial support through the PhD grant of Corentin Pigot (ANR-17-CE08-0010 DUALITY project).

References

[1] Bureš F. Fundamental aspects of property tuning in push–pull molecules. RSC Adv 2014;4:58826–51. https://doi.org/10.1039/C4RA11264D.
[2] Kulhánek J, Bureš F, Pytela O, Mikysek T, Ludvík J, Růžička A. Push-pull molecules with a systematically extended π-conjugated system featuring 4,5-dicyanoimidazole. Dyes and Pigments 2010;85:57–65. https://doi.org/10.1016/j.dyepig.2009.10.004.
[3] Heyer E, Ziessel R. Panchromatic Push–Pull Dyes of Elongated Form from Triphenylamine, Diketopyrrolopyrrole, and Tetracyanobutadiene Modules. Synlett 2015;26:2109–16. https://doi.org/10.1055/s-0034-1378818.
[4] Gómez Esteban S, de la Cruz P, Aljarilla A, Arellano LM, Langa F. Panchromatic Push–Pull Chromophores based on Triphenylamine as Donors for Molecular Solar Cells. Org Lett 2011;13:5362–5. https://doi.org/10.1021/ol202242j.
[5] Duan T, Liang R-Z, Pai Y-F, Wang K, Zhong C, Lu S, et al. Facile synthesis of bis-dicyanovinylidene-end-capped push-pull molecules as panchromatic absorbers. Dyes and Pigments 2019;161:227–32. https://doi.org/10.1016/j.dyepig.2018.09.060.
[6] Huo F, Zhang H, Chen Z, Qiu L, Liu J, Bo S, et al. Novel nonlinear optical push–pull fluorene dyes chromophore as promising materials for telecommunications. J Mater Sci: Mater Electron 2019;30:12180–5. https://doi.org/10.1007/s10854-019-01576-7.
[7] Raimundo J-M, Blanchard P, Gallego-Planas N, Mercier N, Ledoux-Rak I, Hierle R, et al. Design and Synthesis of Push−Pull Chromophores for Second-Order Nonlinear Optics Derived from Rigidified Thiophene-Based π-Conjugating Spacers. J Org Chem 2002;67:205–18. https://doi.org/10.1021/jo010713f.
[8] Mohammed N, Wiles AA, Belsley M, Fernandes SSM, Cariello M, Rotello VM, et al. Synthesis and characterisation of push–pull flavin dyes with efficient second harmonic generation (SHG) properties. RSC Adv 2017;7:24462–9. https://doi.org/10.1039/C7RA03400H.
[9] Parsa Z, Naghavi SS, Safari N. Designing Push–Pull Porphyrins for Efficient Dye-Sensitized Solar Cells. J Phys Chem A 2018;122:5870–7. https://doi.org/10.1021/acs.jpca.8b03668.
[10] Yella A, Mai C-L, Zakeeruddin SM, Chang S-N, Hsieh C-H, Yeh C-Y, et al. Molecular Engineering of Push–Pull Porphyrin Dyes for Highly Efficient Dye-Sensitized Solar Cells: The Role of Benzene Spacers. Angewandte Chemie International Edition 2014;53:2973–7. https://doi.org/10.1002/anie.201309343.
[11] Farré Y, Raissi M, Fihey A, Pellegrin Y, Blart E, Jacquemin D, et al. Synthesis and properties of new benzothiadiazole-based push-pull dyes for p-type dye sensitized solar cells. Dyes and Pigments 2018;148:154–66. https://doi.org/10.1016/j.dyepig.2017.08.055.
[12] Magaldi D, Ulfa M, Péralta S, Goubard F, Pauporté T, Bui T-T. Carbazole-based material: synthesis, characterization, and application as hole transporting material in perovskite solar cells. J Mater Sci: Mater Electron 2021;32:12856–61. https://doi.org/10.1007/s10854-020-04021-2.

[13] Le HT, Saleah R, Kungwan N, Nghiem M-P, Goubard F, Bui T-T. Synthesis, Thermal, Optical and Electrochemical Properties of Acridone and Thioxanthone Based Push-Pull Molecules. ChemistrySelect 2020;5:15180–9. https://doi.org/10.1002/slct.202003376.
[14] Magaldi D, Ulfa M, Péralta S, Goubard F, Pauporté T, Bui T-T. Carbazole Electroactive Amorphous Molecular Material: Molecular Design, Synthesis, Characterization and Application in Perovskite Solar Cells. Energies 2020;13. https://doi.org/10.3390/en13112897.
[15] Magaldi D, Ulfa M, Nghiêm M-P, Sini G, Goubard F, Pauporté T, et al. Hole transporting materials for perovskite solar cells: molecular versus polymeric carbazole-based derivatives. J Mater Sci 2020;55:4820–9. https://doi.org/10.1007/s10853-019-04342-6.
[16] Thooft AM, Cassaidy K, VanVeller B. A Small Push–Pull Fluorophore for Turn-on Fluorescence. J Org Chem 2017;82:8842–7. https://doi.org/10.1021/acs.joc.7b00939.
[17] Karpenko IA, Niko Y, Yakubovskyi VP, Gerasov AO, Bonnet D, Kovtun YP, et al. Push–pull dioxaborine as fluorescent molecular rotor: far-red fluorogenic probe for ligand–receptor interactions. J Mater Chem C 2016;4:3002–9. https://doi.org/10.1039/C5TC03411F.
[18] Jousselin-Oba T, Mamada M, Wright K, Marrot J, Adachi C, Yassar A, et al. Synthesis, Aromaticity, and Application of peri-Pentacenopentacene: Localized Representation of Benzenoid Aromatic Compounds. Angewandte Chemie International Edition 2022;61:e202112794. https://doi.org/10.1002/anie.202112794.
[19] Jousselin-Oba T, Mamada M, Okazawa A, Marrot J, Ishida T, Adachi C, et al. Modulating the ground state, stability and charge transport in OFETs of biradicaloid hexahydro-diindenopyrene derivatives and a proposed method to estimate the biradical character. Chem Sci 2020;11:12194–205. https://doi.org/10.1039/D0SC04583G.
[20] Jousselin-Oba T, Mamada M, Marrot J, Maignan A, Adachi C, Yassar A, et al. Excellent Semiconductors Based on Tetracenotetracene and Pentacenopentacene: From Stable Closed-Shell to Singlet Open-Shell. J Am Chem Soc 2019;141:9373–81. https://doi.org/10.1021/jacs.9b03488.
[21] Jousselin-Oba T, Deal PE, Fix AG, Frederickson CK, Vonnegut CL, Yassar A, et al. Synthesis and Properties of Benzo-Fused Indeno[2,1-c]fluorenes. Chemistry – An Asian Journal 2019;14:1737–44. https://doi.org/10.1002/asia.201801684.
[22] Broman SL, Andersen CL, Jousselin-Oba T, Mansø M, Hammerich O, Frigoli M, et al. Tetraceno[2,1,12,11-opqra]tetracene-extended tetrathiafulvalene – redox-controlled generation of a large PAH core. Org Biomol Chem 2017;15:807–11. https://doi.org/10.1039/C6OB02666D.
[23] Sbargoud K, Mamada M, Jousselin-Oba T, Takeda Y, Tokito S, Yassar A, et al. Low Bandgap Bistetracene-Based Organic Semiconductors Exhibiting Air Stability, High Aromaticity and Mobility. Chemistry – A European Journal 2017;23:5076–80. https://doi.org/10.1002/chem.201605906.
[24] Sbargoud K, Mamada M, Marrot J, Tokito S, Yassar A, Frigoli M. Diindeno[1,2-b:2′,1′-n]perylene: a closed shell related Chichibabin's hydrocarbon, the synthesis, molecular packing, electronic and charge transport properties. Chem Sci 2015;6:3402–9. https://doi.org/10.1039/C5SC00652J.
[25] Tanaka M, Nakamura M, Salhin MAA, Ikeda T, Kamada K, Ando H, et al. Synthesis and Photochromism of Spirobenzopyran Derivatives Bearing an Oxymethylcrown Ether Moiety: Metal Ion-Induced Switching between Positive and Negative Photochromisms. J Org Chem 2001;66:1533–7. https://doi.org/10.1021/jo0013756.
[26] Frigoli M, Marrot J, Gentili PL, Jacquemin D, Vagnini M, Pannacci D, et al. P-Type Photochromism of New Helical Naphthopyrans: Synthesis and Photochemical,

Photophysical and Theoretical Study. ChemPhysChem 2015;16:2447–58. https://doi.org/10.1002/cphc.201500251.
[27] Ishiguro Y, Frigoli M, Hayakawa R, Chikyow T, Wakayama Y. Improved thermal stability in photochromism-based optically controllable organic thin film transistor. Organic Electronics 2014;15:1891–5. https://doi.org/10.1016/j.orgel.2014.05.030.
[28] Frigoli M, Maurel F, Berthet J, Delbaere S, Marrot J, Oliveira MariaM. The Control of Photochromism of [3H]-Naphthopyran Derivatives with Intramolecular CH−π Bonds. Org Lett 2012;14:4150–3. https://doi.org/10.1021/ol301812e.
[29] Delbaere S, Micheau J-C, Frigoli M, Mehl GH, Vermeersch G. Mechanistic understanding of the photochromism of a hybrid dithienylethene–naphthopyran system by NMR spectroscopy. Journal of Physical Organic Chemistry 2007;20:929–35. https://doi.org/10.1002/poc.1188.
[30] Sun K, Pigot C, Zhang Y, Borjigin T, Morlet-Savary F, Graff B, et al. Sunlight Induced Polymerization Photoinitiated by Novel Push–Pull Dyes: Indane-1,3-Dione, 1H-Cyclopenta[b]Naphthalene-1,3(2H)-Dione and 4-Dimethoxyphenyl-1-Allylidene Derivatives. Macromolecular Chemistry and Physics 2022;n/a:2100439. https://doi.org/10.1002/macp.202100439.
[31] Pigot C, Noirbent G, Brunel D, Dumur F. Recent advances on push–pull organic dyes as visible light photoinitiators of polymerization. European Polymer Journal 2020;133:109797. https://doi.org/10.1016/j.eurpolymj.2020.109797.
[32] Zhao J, Lalevée J, Lu H, MacQueen R, Kable SH, Schmidt TW, et al. A new role of curcumin: as a multicolor photoinitiator for polymer fabrication under household UV to red LED bulbs. Polym Chem 2015;6:5053–61. https://doi.org/10.1039/C5PY00661A.
[33] Lalevée J, Blanchard N, Tehfe MA, Fries C, Morlet-Savary F, Gigmes D, et al. New thioxanthone and xanthone photoinitiators based on silyl radical chemistry. Polym Chem 2011;2:1077–84. https://doi.org/10.1039/C0PY00392A.
[34] Belon C, Allonas X, Croutxé-barghorn C, Lalevée J. Overcoming the oxygen inhibition in the photopolymerization of acrylates: A study of the beneficial effect of triphenylphosphine. Journal of Polymer Science Part A: Polymer Chemistry 2010;48:2462–9. https://doi.org/10.1002/pola.24017.
[35] Telitel S, Schweizer S, Morlet-Savary F, Graff B, Tschamber T, Blanchard N, et al. Soft Photopolymerizations Initiated by Dye-Sensitized Formation of NHC-Boryl Radicals under Visible Light. Macromolecules 2013;46:43–8. https://doi.org/10.1021/ma302009p.
[36] Lalevée J, Fouassier JP. Recent advances in sunlight induced polymerization: role of new photoinitiating systems based on the silyl radical chemistry. Polym Chem 2011;2:1107–13. https://doi.org/10.1039/C1PY00073J.
[37] Lalevée J, Telitel S, Tehfe MA, Fouassier JP, Curran DP, Lacôte E. N-Heterocyclic Carbene Boranes Accelerate Type I Radical Photopolymerizations and Overcome Oxygen Inhibition. Angewandte Chemie International Edition 2012;51:5958–61.
[38] Garra P, Graff B, Morlet-Savary F, Dietlin C, Becht J-M, Fouassier J-P, et al. Charge Transfer Complexes as Pan-Scaled Photoinitiating Systems: From 50 μm 3D Printed Polymers at 405 nm to Extremely Deep Photopolymerization (31 cm). Macromolecules 2018;51:57–70. https://doi.org/10.1021/acs.macromol.7b02185.
[39] Fouassier JP, Lalevée J. Three-component photoinitiating systems: towards innovative tailor made high performance combinations. RSC Adv 2012;2:2621–9. https://doi.org/10.1039/C2RA00892K.
[40] Ravelli D, Fagnoni M. Dyes as Visible Light Photoredox Organocatalysts. ChemCatChem 2012;4:169–71. https://doi.org/10.1002/cctc.201100363.

[41] Le T, Courant T, Merad J, Allain C, Audebert P, Masson G. s-Tetrazine Dyes: A Facile Generation of Photoredox Organocatalysts for Routine Oxidations. J Org Chem 2019;84:16139–46. https://doi.org/10.1021/acs.joc.9b02454.
[42] Fidaly K, Ceballos C, Falguières A, Veitia MS-I, Guy A, Ferroud C. Visible light photoredox organocatalysis: a fully transition metal-free direct asymmetric α-alkylation of aldehydes. Green Chem 2012;14:1293–7. https://doi.org/10.1039/C2GC35118H.
[43] Oliveira V da G, Cardoso MF do C, Forezi L da SM. Organocatalysis: A Brief Overview on Its Evolution and Applications. Catalysts 2018;8:605. https://doi.org/10.3390/catal8120605.
[44] Dietlin C, Schweizer S, Xiao P, Zhang J, Morlet-Savary F, Graff B, et al. Photopolymerization upon LEDs: new photoinitiating systems and strategies. Polym Chem 2015;6:3895–912. https://doi.org/10.1039/C5PY00258C.
[45] Tehfe MA, Louradour F, Lalevée J, Fouassier J-P. Photopolymerization Reactions: On the Way to a Green and Sustainable Chemistry. Applied Sciences 2013;3:490–514. https://doi.org/10.3390/app3020490.
[46] Lalevée J, Mokbel H, Fouassier J-P. Recent Developments of Versatile Photoinitiating Systems for Cationic Ring Opening Polymerization Operating at Any Wavelengths and under Low Light Intensity Sources. Molecules 2015;20:7201–21. https://doi.org/10.3390/molecules20047201.
[47] Tehfe MA, Lalevée J, Allonas X, Fouassier JP. Long Wavelength Cationic Photopolymerization in Aerated Media: A Remarkable Titanocene/Tris(trimethylsilyl)silane/Onium Salt Photoinitiating System. Macromolecules 2009;42:8669–74. https://doi.org/10.1021/ma9016696.
[48] Guillaneuf Y, Versace D-L, Bertin D, Lalevée J, Gigmes D, Fouassier J-P. Importance of the Position of the Chromophore Group on the Dissociation Process of Light Sensitive Alkoxyamines. Macromolecular Rapid Communications 2010;31:1909–13. https://doi.org/10.1002/marc.201000316.
[49] Fouassier JP, Allonas X, Lalevee J, Visconti M. Radical polymerization activity and mechanistic approach in a new three-component photoinitiating system. Journal of Polymer Science Part A: Polymer Chemistry 2000;38:4531–41. https://doi.org/10.1002/1099-0518(20001215)38:24<4531::AID-POLA220>3.0.CO;2-U.
[50] Zhang J, Lalevée J, Zhao J, Graff B, Stenzel MH, Xiao P. Dihydroxyanthraquinone derivatives: natural dyes as blue-light-sensitive versatile photoinitiators of photopolymerization. Polym Chem 2016;7:7316–24. https://doi.org/10.1039/C6PY01550F.
[51] Quint V, Chouchène N, Askri M, Lalevée J, Gaumont A-C, Lakhdar S. Visible-light-mediated α-phosphorylation of N-aryl tertiary amines through the formation of electron-donor–acceptor complexes: synthetic and mechanistic studies. Org Chem Front 2019;6:41–4. https://doi.org/10.1039/C8QO00985F.
[52] Tehfe M-A, Lalevée J, Morlet-Savary F, Blanchard N, Fries C, Graff B, et al. Near UV–visible light induced cationic photopolymerization reactions: A three component photoinitiating system based on acridinedione/silane/iodonium salt. European Polymer Journal 2010;46:2138–44. https://doi.org/10.1016/j.eurpolymj.2010.09.014.
[53] Kuhn H. Oscillator Strength of Absorption Band in Dye Molecules. J Chem Phys 1958;29:958–9. https://doi.org/10.1063/1.1744627.
[54] Feng J, Jiao Y, Ma W, Nazeeruddin MdK, Grätzel M, Meng S. First Principles Design of Dye Molecules with Ullazine Donor for Dye Sensitized Solar Cells. J Phys Chem C 2013;117:3772–8. https://doi.org/10.1021/jp310504n.

[55] Coe BJ, Rusanova D, Joshi VD, Sánchez S, Vávra J, Khobragade D, et al. Helquat Dyes: Helicene-like Push–Pull Systems with Large Second-Order Nonlinear Optical Responses. J Org Chem 2016;81:1912–20. https://doi.org/10.1021/acs.joc.5b02692.
[56] Francos J, García-Garrido SE, Borge J, Suárez FJ, Cadierno V. Butadiene dyes based on 3-(dicyanomethylidene)indan-1-one and 1,3-bis(dicyanomethylidene)indane: synthesis, characterization and solvatochromic behaviour. RSC Adv 2016;6:6858–67. https://doi.org/10.1039/C5RA27005G.
[57] Jang S-R, Lee C, Choi H, Ko JJ, Lee J, Vittal R, et al. Oligophenylenevinylene-Functionalized Ru(II)-bipyridine Sensitizers for Efficient Dye-Sensitized Nanocrystalline TiO2 Solar Cells. Chem Mater 2006;18:5604–8. https://doi.org/10.1021/cm061447v.
[58] Shandura MP, Poronik YM, Kovtun YP. Substituted xanthylocyanines. II. Pyroninocyanines. Dyes and Pigments 2005;66:171–7. https://doi.org/10.1016/j.dyepig.2004.09.011.
[59] Sun K, Liu S, Pigot C, Brunel D, Graff B, Nechab M, et al. Novel Push–Pull Dyes Derived from 1H-cyclopenta[b]naphthalene-1,3(2H)-dione as Versatile Photoinitiators for Photopolymerization and Their Related Applications: 3D Printing and Fabrication of Photocomposites. Catalysts 2020;10:1196. https://doi.org/10.3390/catal10101196.
[60] Sun K, Pigot C, Chen H, Nechab M, Gigmes D, Morlet-Savary F, et al. Free Radical Photopolymerization and 3D Printing Using Newly Developed Dyes: Indane-1,3-Dione and 1H-Cyclopentanaphthalene-1,3-Dione Derivatives as Photoinitiators in Three-Component Systems. Catalysts 2020;10:463. https://doi.org/10.3390/catal10040463.
[61] Tehfe M-A, Dumur F, Graff B, Morlet-Savary F, Fouassier J-P, Gigmes D, et al. New Push–Pull Dyes Derived from Michler's Ketone For Polymerization Reactions Upon Visible Lights. Macromolecules 2013;46:3761–70. https://doi.org/10.1021/ma400766z.
[62] Kavalli T, Wolf R, Ozen S, Lalevée J. Comparison of pure epoxy vs. epoxy-anhydride photopolymerization. European Polymer Journal 2022;166:111031. https://doi.org/10.1016/j.eurpolymj.2022.111031.
[63] Kavalli T, Wolf R, Lalevée J. Ultrafast Epoxy-Anhydride Photopolyaddition Reaction. Macromolecular Chemistry and Physics 2020;221:2000236. https://doi.org/10.1002/macp.202000236.
[64] Kirschner J, Baralle A, Paillard J, Graff B, Becht J-M, Klee JE, et al. Silyl Glyoximides: Toward a New Class of Visible Light Photoinitiators. Macromolecular Chemistry and Physics 2022;223:2100500. https://doi.org/10.1002/macp.202100500.
[65] Topa-Skwarczyńska M, Galek M, Jankowska M, Morlet-Savary F, Graff B, Lalevée J, et al. Development of the first panchromatic BODIPY-based one-component iodonium salts for initiating the photopolymerization processes. Polym Chem 2021;12:6873–93. https://doi.org/10.1039/D1PY01263K.
[66] Hammoud F, Lee Z-H, Graff B, Hijazi A, Lalevée J, Chen Y-C. Novel phenylamine-based oxime ester photoinitiators for LED-induced free radical, cationic, and hybrid polymerization. Journal of Polymer Science 2021;59:1711–23. https://doi.org/10.1002/pol.20210298.
[67] Zhang Y, Liu S, Chen H, Josien L, Schrodj G, Simon-Masseron A, et al. Development of a Zeolite/Polymer-Based Hydrogel Composite through Photopolymerization for 3D Printing Application. Macromolecular Materials and Engineering 2021;306:2100129. https://doi.org/10.1002/mame.202100129.
[68] Gencoglu T, Graff B, Morlet-Savary F, Lalevée J, Avci D. Benzophenone-Functionalized Oligo(Amido Amine)/Iodonium Salt Systems as Visible Light Photoinitiators. ChemistrySelect 2021;6:5743–51. https://doi.org/10.1002/slct.202100991.

[69] Zhang Y, Chen H, Liu S, Josien L, Schrodj G, Simon-Masseron A, et al. Photopolymerization of Pollen Based Biosourced Composites and Applications in 3D and 4D Printing. Macromolecular Materials and Engineering 2021;306:2000774. https://doi.org/10.1002/mame.202000774.
[70] Lai H, Zhu D, Peng X, Zhang J, Lalevée J, Xiao P. N-Aryl glycines as versatile initiators for various polymerizations. Polym Chem 2021;12:1991–2000. https://doi.org/10.1039/D1PY00030F.
[71] Zeng B, Cai Z, Lalevée J, Yang Q, Lai H, Xiao P, et al. Cytotoxic and cytocompatible comparison among seven photoinitiators-triggered polymers in different tissue cells. Toxicology in Vitro 2021;72:105103. https://doi.org/10.1016/j.tiv.2021.105103.
[72] Sprick E, Becht J-M, Graff B, Salomon J-P, Tigges T, Weber C, et al. New hydrogen donors for amine-free photoinitiating systems in dental materials. Dental Materials 2021;37:382–90. https://doi.org/10.1016/j.dental.2020.12.013.
[73] Ghanem T, Vincendeau T, Marqués PS, Habibi AH, Abidi S, Yassin A, et al. Synthesis of push–pull triarylamine dyes containing 5,6-difluoro-2,1,3-benzothiadiazole units by direct arylation and their evaluation as active material for organic photovoltaics. Mater Adv 2021;2:7456–62. https://doi.org/10.1039/D1MA00798J.
[74] Jin-Woo Choi, Kim C-H, Pison J, Oyedele A, Denis Tondelier, Antoine Leliège, et al. Exploiting the potential of 2-((5-(4-(diphenylamino)phenyl)thiophen-2-yl)methylene)malononitrile as an efficient donor molecule in vacuum-processed bulk-heterojunction organic solar cells. Rsc Advances 2014;4:5236–42.
[75] Kotowicz S, Sęk D, Kula S, Fabiańczyk A, Siwy M, Filapek M, et al. Malononitrile derivatives as push-pull molecules: Structure - properties relationships characterization. Journal of Luminescence 2018;203:455–66. https://doi.org/10.1016/j.jlumin.2018.06.071.
[76] Bogdanov G, Tillotson JP, Khrustalev VN, Rigin S, Timofeeva TV. Synthesis, crystal structure studies and solvatochromic behaviour of two 2-5-[4-(di\-methyl\-amino)\-phen\-yl]penta-2,4-dien-1-yl\-idenemalono\-nitrile derivatives. Acta Crystallographica Section C 2019;75:1175–81. https://doi.org/10.1107/S2053229619010398.
[77] Deligeorgiev T, Vasilev A, Kaloyanova S, Vaquero JJ. Styryl dyes – synthesis and applications during the last 15 years. Coloration Technology 2010;126:55–80. https://doi.org/10.1111/j.1478-4408.2010.00235.x.
[78] Narang U, Zhao CF, Bhawalkar JD, Bright FV, Prasad PN. Characterization of a New Solvent-Sensitive Two-Photon-Induced Fluorescent (Aminostyryl)pyridinium Salt Dye. J Phys Chem 1996;100:4521–5. https://doi.org/10.1021/jp953367c.
[79] Wong JJH, Wright SK, Ghozalli I, Mehra R, Furuya K, Katayama DS. Simultaneous High-Throughput Conformational and Colloidal Stability Screening Using a Fluorescent Molecular Rotor Dye, 4-(4-(Dimethylamino)styryl)-N-Methylpyridinium Iodide (DASPMI). J Biomol Screen 2016;21:842–50. https://doi.org/10.1177/1087057116646553.
[80] Dalessandro EV, Collin HP, Guimarães LGL, Valle MS, Pliego JR. Mechanism of the Piperidine-Catalyzed Knoevenagel Condensation Reaction in Methanol: The Role of Iminium and Enolate Ions. J Phys Chem B 2017;121:5300–7. https://doi.org/10.1021/acs.jpcb.7b03191.
[81] van Beurden K, de Koning S, Molendijk D, van Schijndel J. The Knoevenagel reaction: a review of the unfinished treasure map to forming carbon–carbon bonds. Null 2020;13:349–64. https://doi.org/10.1080/17518253.2020.1851398.
[82] Pigot C, Noirbent G, Peralta S, Duval S, Nechab M, Gigmes D, et al. Unprecedented Nucleophilic Attack of Piperidine on the Electron Acceptor during the Synthesis of

Push-Pull Dyes by a Knoevenagel Reaction. Helvetica Chimica Acta 2019;102:e1900229. https://doi.org/10.1002/hlca.201900229.
[83] Pigot C, Noirbent G, Bui T-T, Péralta S, Duval S, Nechab M, et al. Synthesis, optical and electrochemical properties of a series of push-pull dyes based on the 4,4-bis(4-methoxy phenyl)butadienyl donor. Dyes and Pigments 2021;194:109552. https://doi.org/10.1016/j.dyepig.2021.109552.
[84] Noirbent G, Pigot C, Bui T-T, Péralta S, Nechab M, Gigmes D, et al. Dyes with tunable absorption properties from the visible to the near infrared range: 2,4,5,7-Tetranitrofluorene (TNF) as a unique electron acceptor. Dyes and Pigments 2021;189:109250. https://doi.org/10.1016/j.dyepig.2021.109250.
[85] Noirbent G, Pigot C, Bui T-T, Péralta S, Nechab M, Gigmes D, et al. Synthesis, optical and electrochemical properties of a series of push-pull dyes based on the 2-(3-cyano-4,5,5-trimethylfuran-2(5H)-ylidene)malononitrile (TCF) acceptor. Dyes and Pigments 2021;184:108807. https://doi.org/10.1016/j.dyepig.2020.108807.
[86] Dumur F, Mayer CR, Dumas E, Miomandre F, Frigoli M, Sécheresse F. New Chelating Stilbazonium-Like Dyes from Michler's Ketone. Org Lett 2008;10:321–4. https://doi.org/10.1021/ol702793j.
[87] Wössner JS, Esser B. Spiroconjugated Donor−σ–Acceptor Charge-Transfer Dyes: Effect of the π-Subsystems on the Optoelectronic Properties. J Org Chem 2020;85:5048–57. https://doi.org/10.1021/acs.joc.0c00567.
[88] Yang X, Fox T, Berke H. Synthetic and mechanistic studies of metal-free transfer hydrogenations applying polarized olefins as hydrogen acceptors and amine borane adducts as hydrogen donors. Org Biomol Chem 2012;10:852–60. https://doi.org/10.1039/C1OB06381B.
[89] Morales AR, Frazer A, Woodward AW, Ahn-White H-Y, Fonari A, Tongwa P, et al. Design, Synthesis, and Structural and Spectroscopic Studies of Push–Pull Two-Photon Absorbing Chromophores with Acceptor Groups of Varying Strength. J Org Chem 2013;78:1014–25. https://doi.org/10.1021/jo302423p.
[90] Planells M, Robertson N. Naphthyl Derivatives Functionalised with Electron Acceptor Units – Synthesis, Electronic Characterisation and DFT Calculations. European Journal of Organic Chemistry 2012;2012:4947–53. https://doi.org/10.1002/ejoc.201200715.
[91] Marvi Omid, Giahi Masoud. Montmorillonite KSF Clay as Novel and Recyclable Heterogeneous Catalyst for the Microwave Mediated Synthesis of Indan-1,3-Diones. Bulletin of the Korean Chemical Society 2009;30:2918–20. https://doi.org/10.5012/BKCS.2009.30.12.2918.
[92] Hark RR, Hauze DB, Petrovskaia O, Joullié MM, Jaouhari R, McComiskey P. Novel approaches toward ninhydrin analogs. Tetrahedron Letters 1994;35:7719–22. https://doi.org/10.1016/0040-4039(94)80101-0.
[93] Noirbent G, Dumur F. Recent Advances on Nitrofluorene Derivatives: Versatile Electron Acceptors to Create Dyes Absorbing from the Visible to the Near and Far Infrared Region. Materials 2018;11:2425. https://doi.org/10.3390/ma11122425.
[94] Frisch MJ, Trucks GW, Schlegel HB, Scuseria GE, Robb MA, Cheeseman JR, et al. Gaussian 16 Rev. C.01. Wallingford, CT: 2016.
[95] Lee C, Yang W, Parr RG. Development of the Colle-Salvetti correlation-energy formula into a functional of the electron density. Phys Rev B 1988;37:785–9. https://doi.org/10.1103/PhysRevB.37.785.
[96] Becke AD. A new mixing of Hartree–Fock and local density-functional theories. J Chem Phys 1993;98:1372–7. https://doi.org/10.1063/1.464304.
[97] Hehre WJ, Ditchfield R, Pople JA. Self—Consistent Molecular Orbital Methods. XII. Further Extensions of Gaussian—Type Basis Sets for Use in Molecular Orbital Studies

of Organic Molecules. J Chem Phys 1972;56:2257–61. https://doi.org/10.1063/1.1677527.
[98] Scalmani G, Frisch MJ. Continuous surface charge polarizable continuum models of solvation. I. General formalism. J Chem Phys 2010;132:114110. https://doi.org/10.1063/1.3359469.
[99] O'boyle NM, Tenderholt AL, Langner KM. cclib: A library for package-independent computational chemistry algorithms. Journal of Computational Chemistry 2008;29:839–45. https://doi.org/10.1002/jcc.20823.
[100] Tomasi J, Mennucci B, Cancès E. The IEF version of the PCM solvation method: an overview of a new method addressed to study molecular solutes at the QM ab initio level. Journal of Molecular Structure: THEOCHEM 1999;464:211–26. https://doi.org/10.1016/S0166-1280(98)00553-3.
[101] Guerrini M, Cocchi C, Calzolari A, Varsano D, Corni S. Interplay between Intra- and Intermolecular Charge Transfer in the Optical Excitations of J-Aggregates. J Phys Chem C 2019;123:6831–8. https://doi.org/10.1021/acs.jpcc.8b11709.
[102] Kamlet MJ, Abboud JLM, Abraham MH, Taft RW. Linear solvation energy relationships. 23. A comprehensive collection of the solvatochromic parameters, .pi.*, .alpha., and .beta., and some methods for simplifying the generalized solvatochromic equation. J Org Chem 1983;48:2877–87. https://doi.org/10.1021/jo00165a018.
[103] Catalán J. On the ET (30), π*, Py, S', and SPP Empirical Scales as Descriptors of Nonspecific Solvent Effects. J Org Chem 1997;62:8231–4. https://doi.org/10.1021/jo971040x.
[104] Kawski A. der Wellenzahl von elecktronenbanden lumineszierenden molecule. Acta Phys Polon 1966;29:507–18.
[105] Lippert E. Dipolmoment und Elektronenstruktur von angeregten Molekülen. Zeitschrift Für Naturforschung A 1955;10:541–5. https://doi.org/10.1515/zna-1955-0707.
[106] Suppan P. Solvent effects on the energy of electronic transitions: experimental observations and applications to structural problems of excited molecules. J Chem Soc A 1968:3125–33. https://doi.org/10.1039/J19680003125.
[107] Reichardt C. Solvatochromic Dyes as Solvent Polarity Indicators. Chem Rev 1994;94:2319–58. https://doi.org/10.1021/cr00032a005.
[108] Bakshiev NG. Universal intermolecular interactions and their effect on the position of the electronic spectra of molecules in two component solutions. Optika i Spektroskopiya 1964;16:821–32.
[109] Bauer M, Rollberg A, Barth A, Spange S. Differentiating Between Dipolarity and Polarizability Effects of Solvents Using the Solvatochromism of Barbiturate Dyes. European Journal of Organic Chemistry 2008;2008:4475–81. https://doi.org/10.1002/ejoc.200800355.
[110] Jessop PG, Jessop DA, Fu D, Phan L. Solvatochromic parameters for solvents of interest in green chemistry. Green Chem 2012;14:1245–59. https://doi.org/10.1039/C2GC16670D.
[111] Ooyama Y, Asada R, Inoue S, Komaguchi K, Imae I, Harima Y. Solvatochromism of novel donor–π–acceptor type pyridinium dyes in halogenated and non-halogenated solvents. New J Chem 2009;33:2311–6. https://doi.org/10.1039/B9NJ00332K.
[112] Rezende MC, Aracena A. A general framework for the solvatochromism of pyridinium phenolate betaine dyes. Chemical Physics Letters 2013;558:77–81. https://doi.org/10.1016/j.cplett.2012.09.067.
[113] Jacques P, Graff B, Diemer V, Ay E, Chaumeil H, Carré C, et al. Negative solvatochromism of a series of pyridinium phenolate betaine dyes with increasing steric

hindrance. Chemical Physics Letters 2012;531:242–6. https://doi.org/10.1016/j.cplett.2012.02.018.
[114] Pommerehne J, Vestweber H, Guss W, Mahrt RF, Bässler H, Porsch M, et al. Efficient two layer leds on a polymer blend basis. Advanced Materials 1995;7:551–4. https://doi.org/10.1002/adma.19950070608.
[115] Cardona CM, Li W, Kaifer AE, Stockdale D, Bazan GC. Electrochemical Considerations for Determining Absolute Frontier Orbital Energy Levels of Conjugated Polymers for Solar Cell Applications. Advanced Materials 2011;23:2367–71. https://doi.org/10.1002/adma.201004554.